X-ray microbeam measurements of individual dislocation cell elastic strains in deformed single-crystal copper

LYLE E. LEVINE[1]*, BENNETT C. LARSON[2], WENGE YANG[3], MICHAEL E. KASSNER[4], JONATHAN Z. TISCHLER[2], MICHAEL A. DELOS-REYES[4], RICHARD J. FIELDS[1] AND WENJUN LIU[5]

[1]Materials Science & Engineering Laboratory, National Institute of Standards and Technology, Gaithersburg, Maryland 20899-8553, USA
[2]Materials Science & Technology Division, Oak Ridge National Laboratory, Oak Ridge, Tennessee 37831, USA
[3]HPCAT/Carnegie Institution of Washington, Advanced Photon Source, Argonne National Laboratory, Argonne, Illinois 60439, USA
[4]Department of Aerospace and Mechanical Engineering, University of Southern California, Los Angeles, California 90089, USA
[5]Advanced Photon Source, Argonne National Laboratory, Argonne, Illinois 60439-4800, USA
*e-mail: Lyle.Levine@nist.gov

Published online: 16 July 2006; doi:10.1038/nmat1698

The distribution of elastic strains (and thus stresses) at the submicrometre length scale within deformed metal single crystals has remarkably broad implications for our understanding of important physical phenomena. These include the evolution of the complex dislocation structures that govern mechanical behaviour within individual grains[1–3], the transport of dislocations through such structures[4–6], changes in mechanical properties that occur during reverse loading[7–9] (for example, sheet-metal forming and fatigue), and the analyses of diffraction line profiles for microstructural studies of these phenomena[10–15]. We present the first direct, spatially resolved measurements of the elastic strains within individual dislocation cells in copper single crystals deformed in tension and compression along ⟨001⟩ axes. Broad distributions of elastic strains are found, with important implications for theories of dislocation structure evolution[3,16–20], dislocation transport[4–6], and the extraction of dislocation parameters from X-ray line profiles[10–15,21–24].

The formation and evolution of dislocation cell structures (patterning) is one of the most important aspects of the deformation process in ductile metals[1–3,17–20]. It is generally appreciated that patterning arises from the collective interactions of dislocations[4,5,16–20] and recent *in situ* diffraction-resolved measurements have shown crystal lattice breakup starting very early in the deformation process[25]. However, it is not yet possible to predict the evolution of dislocation distributions and the resulting local stresses. The existence, magnitude and spatial distribution of these stresses with respect to the dislocation microstructure have been long debated[7,10,11,15,16,26–28]; a definitive resolution of this issue over the full range of deformation is needed to validate and guide the ongoing development of recent dislocation patterning[3,17–20] and dislocation transport[4–6] theories.

Each of these important issues can be addressed through the use of a local, spatially resolved, experimental probe that measures unambiguously the lattice parameter (that is, elastic strain) within individual subsurface dislocation cells in bulk single crystals. White-beam differential-aperture X-ray microscopy[29] (DAXM) using submicrometre X-ray beams, and in particular its scanning-monochromatic extension[30], exemplify such a local microstructural technique. Whereas white-beam DAXM measures deviatoric (shear) strains with submicrometre resolution in three dimensions, scanning-monochromatic DAXM provides absolute measurements of dilatational lattice parameters, and hence dilatational strains, with 3D submicrometre resolution. We have used this latter technique to probe the lattice strain within individual dislocation cells in copper single crystals deformed uniaxially in tension and compression.

In this letter, axial 006 reflections were used to probe the local elastic lattice strains, ε_{001}, (and thus the stresses) within individual dislocation cells along the axial ⟨001⟩ deformation direction. As shown in Fig. 1 and discussed in the Methods section, spatially resolved DAXM measurements were conducted using a monochromatic X-ray microbeam focused to $\approx 0.5\,\mu m$ (refs 31,32), where the diffracted beams were detected using a charge-coupled device (CCD) area X-ray detector and depth resolution was provided by a diffracted-beam profiler[30]. Before carrying out the spatially resolved lattice spacing measurements, (spatially integrated) X-ray line profiles were measured on both the compression and tension deformed specimens using the XOR/UNI beamline 33-BM at the Advanced Photon Source (APS), as plotted in Fig. 2; similar line-profile measurements on undeformed copper were used to establish the zero position for the scattering vector, $\mathbf{q}$ (where $q = |\mathbf{q}| = (4\pi/\lambda)\sin\theta$, λ is the X-ray wavelength, and θ is the Bragg angle).

The sample image in Fig. 1 is a transmission electron microscope (TEM) micrograph of a ⟨001⟩ copper compression sample strained to 25% true strain. The width of the incident

©2006 Nature Publishing Group

X-ray microbeam (drawn to scale) shows the size of the microbeam relative to the dislocation microstructure, and the dark parallel lines on the microbeam show the depth resolution provided by the diffracted beam (platinum wire) profiler. Local variations in the elastic strain and crystallographic orientation are detected by measuring the changes in both the Bragg energy and the direction of the diffracted beam (Bragg angle). These local variations greatly distort the diffracted X-ray intensity distribution and the CCD face shown in Fig. 1 shows a typical example of the intensity distribution (false colour) for a single reflection from the compression X-ray sample, as obtained by a 200 eV energy scan of the incident microbeam energy. The areas exhibiting high-diffracted X-ray intensity (blue) come primarily from sample volumes in which the diffraction is largely coherent (dislocation cell interiors). In contrast, dislocation cell walls have high dislocation content, producing a wide range of local sample orientations and strains. Diffraction from such sample volumes cannot be highly localized in scattering angle, rather the local disorientations will produce significant smearing of the X-ray intensity (such as the red and yellow areas for instance). However, diffraction from small coherent scattering volumes and finite-size broadening will also contribute smeared scattering, so cell-wall scattering cannot be so readily identified visually. It is important to note in this connection that because step-scanning the platinum wire directly identifies how much of the observed scattering in a given high-intensity (blue) region comes from a single localized sample volume, the DAXM measurements have no significant contamination from dislocation cell walls or other dislocation cells.

For each position of the sample under the microbeam, high-intensity regions on the CCD (from individual dislocation cells) were selected for a scanning monochromatic DAXM analysis. Two-dimensional scans of beam energy versus platinum wire position yielded intensity plots such as that shown in the inset of Fig. 2a, where the grid indicates 2 eV energy steps and 0.5 μm depth steps, projected along the microbeam path. Gaussian functions were fitted to these data, giving both the depth of the originating dislocation cell and the beam energy at the centre of the peak of the 006 rocking curve. As the microbeam energy, the position of the diffracting volume with respect to individual pixels on the CCD area detector, and the incident beam path are all known through the microscope calibration, the local lattice parameter can be determined directly through Bragg's law. The standard deviation uncertainty (shown graphically in the box in Fig. 2b) is estimated to be 1×10^{-4} for the elastic strain measurements.

The solid red lines in Fig. 2a,b show the measured axial 006 X-ray line profiles (spatially integrated) from the compression and tensile samples. These profiles exhibit the well-known asymmetric shape for copper with a high-scattering-angle tail for compression and a low-angle tail for tension[11]. Spatially resolved axial lattice plane spacing (d-spacing) strains (vertical blue lines) measured from individual dislocation cells, using scanning monochromatic DAXM as described above, are also shown. Thus, the vertical blue lines in Fig. 2a,b correspond to the centre in $\Delta q/q$ of the diffraction profiles for each of the individual cell-interior regions measured. As predicted by Mughrabi's well-known two-component composite model for plastic deformation[16], all 12 of the measured d-spacings in the compression sample (Fig. 2a) are shifted to smaller q (larger d-spacing) and all nine of those in the tension sample (Fig. 2b) are shifted to larger q (smaller d-spacing). The mean elastic strains for the compression and tension samples are $(8.5 \pm 1.1) \times 10^{-4}$ and $(-5.2 \pm 0.9) \times 10^{-4}$, respectively (with one standard deviation uncertainties).

These spatially resolved elastic strain measurements provide the first direct, quantitative test of the two-component composite model that is commonly used to extract average cell-interior and cell-wall stresses from broadened X-ray line profiles[10,11,15]. The best comparison with experimental work in the literature is a study by Mughrabi *et al.*[11], corrected as described in ref. 27. There, a copper single crystal was deformed in tension along a ⟨001⟩ axis to a maximum applied stress of 185 MPa (reported as 75.6 MPa resolved shear stress), comparable to our tensile specimen (196 MPa). Measured X-ray line profiles were asymmetric and a subpeak analysis gave an average cell-interior axial stress of −11% (no uncertainty estimates were given) of the flow stress. Given the several assumptions that were required for the analysis, this value compares well with our mean elastic strain of −17% ± 4% of the flow stress, providing crucial quantitative validation of the composite model predictions.

A key finding of the present study, however, is the dramatic variation of these strains from cell to cell within the sample; the full-widths at half-maximum for the tension and compression cases are similar with an average value of $\approx 7.8 \times 10^{-4}$. As can be seen from the quantitative measurements of individual dislocation cell strains shown in Fig. 2a,b, these elastic strains contribute significantly to the shape and width of the diffraction

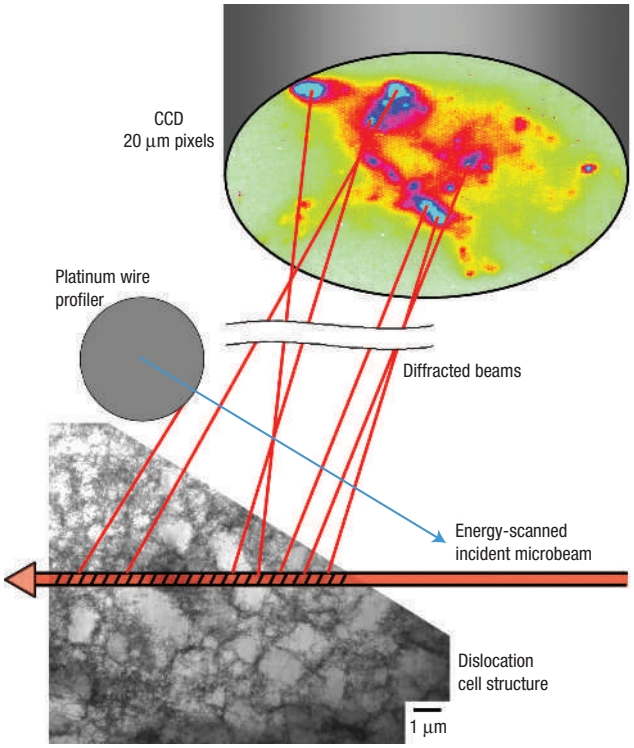

Figure 1 Diagram of the experimental geometry showing how monochromatic differential aperture X-ray microscopy was used in these experiments. TEM micrograph of a single-crystal copper compression sample strained to 25% true strain. The dark regions in the micrograph are high-dislocation-density walls surrounding low-dislocation-density cell interiors. The incident microbeam is drawn to the same scale as the TEM micrograph, showing the 0.5 μm beam size relative to the dislocation microstructure. Diffracted X-ray beams intersect the face of the CCD area detector and the platinum wire profiler provides depth resolution by translating parallel to the sample surface and blocking the diffracted beams. The parallel lines on the incident beam show the 0.5-μm-depth resolution as determined by the 0.7-μm-profiler step size. The CCD face shows a typical integrated X-ray intensity distribution (false colour) for a single X-ray reflection obtained by scanning the X-ray microbeam over 200 eV.

©2006 Nature Publishing Group

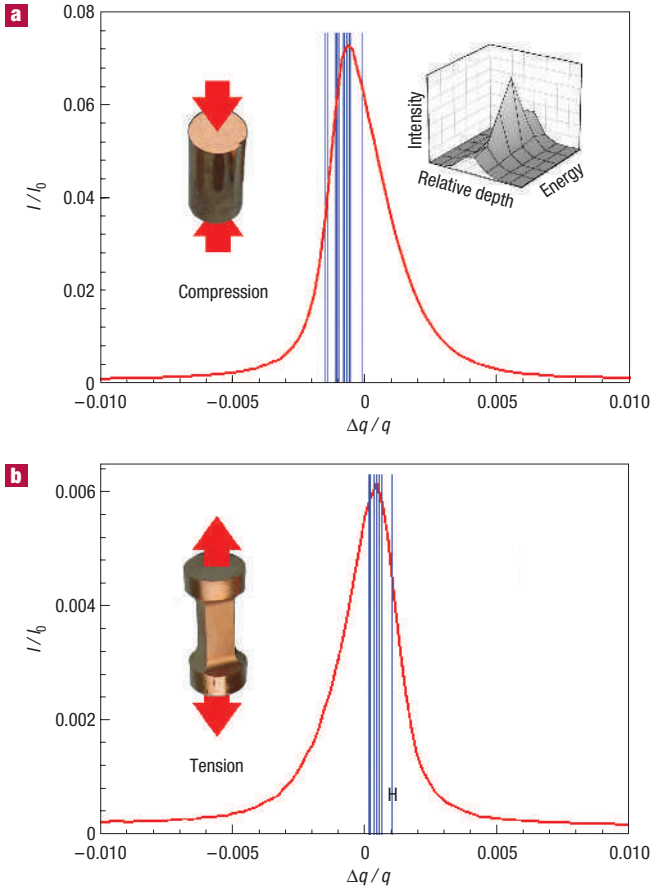

Figure 2 Comparison between spatially integrated and spatially resolved X-ray diffraction experiments on deformed copper single-crystals. **a**, Photograph and X-ray results from the ⟨001⟩ compression specimen. Inset: a representative beam energy and depth scan for a typical dislocation cell, where the energy grid lines denote 2 eV steps, the depth grid lines denote 0.5 μm steps and the centre of the peak determines the 006 Bragg angle for the cell. **b**, Photograph and corresponding results from the ⟨001⟩ tension specimen. The red lines in both panels are spatially averaged axial 006 line profiles obtained using conventional X-ray diffraction techniques. The vertical blue lines in both panels show the corresponding diffraction peak centres from individual dislocation cells, measured using spatially resolved monochromatic differential-aperture X-ray microscopy. The error bar indicates one standard deviation. As predicted by the two-component composite model, the cell strains in **a** are shifted to smaller q and those in **b** are shifted to larger q.

line profiles. Quantitative analyses of extracted cell-wall and cell-interior subpeaks frequently use theoretical descriptions of dislocation broadened line profiles[21–23] to extract dislocation structure parameters from plastically deformed samples. Such analyses often have the tacit assumption that all of the subpeak broadening comes from the dislocations and therefore that cell-to-cell strain variations are negligible, an assumption that must now be re-evaluated in view of these measurements. In addition, as the dislocation cell elastic strains originate as backstresses from the dislocation walls, the observed variation in the cell-interior strains strongly suggest that a similarly broad distribution exists for the dislocation walls themselves. Cell-wall strain distributions will contribute significantly to the width and shape of the line profiles on the asymmetric tail side of the peaks. In principle, the cell-interior and cell-wall strain distribution functions could be removed from the line profile by a deconvolution algorithm, but the profile would first have to be separated into cell-interior and wall subpeaks and the strain distribution functions would have to be known. Fortunately, Groma recently provided a more elegant solution[24] by deriving an asymptotic analytical expression for the tails of a dislocation-broadened line profile. This expression should be largely independent of the actual dislocation distribution and relatively insensitive to the local stress variations reported here.

The existence of a broad distribution of dislocation cell elastic strains also has important implications for theoretical models of dislocation patterning and dislocation transport. At the dislocation level, critically important phenomena such as dislocation bowing, dislocation pinning and unpinning, unzipping of locks, and cross slip are highly sensitive to the local stress field experienced by the dislocations. Thus, theoretical models of dislocation patterning and transport must frequently make assumptions about the distributions of such stresses within a specimen. Converting our measured axial elastic strains to axial stresses using the elastic modulus in the ⟨001⟩ direction, $E_{001} = 66.6 \pm 0.5$ GPa (ref. 33), the stresses range from essentially zero up to 50% of the macroscopic flow stress. Existing dislocation transport models based on dislocation bowing and percolation theory[5,6] that assume such stress variations are negligible will have to be revisited in light of the current findings.

On the other hand, at least one prominent dislocation patterning model bases the entire evolution process on the presence of stress variations such as those reported here. Hähner *et al.* developed a theoretical model of dislocation cell formation[17] to explain the power-law size distribution of dislocation cells in copper single crystals, deformed uniaxially along a ⟨001⟩ axis. The model associates dislocation cell formation with a noise-induced structural transition in a system far from equilibrium, where the noise term reflects fluctuations in the stress experienced by mobile dislocations traversing a sample. Extensions of this model[18–20] relate the stress fluctuations to variations in the local dislocation density and generalize the two-component composite model to account for a continuous spectrum of local dislocation densities and cell stresses. The dislocation cell elastic strain measurements reported here provide striking experimental support for the underlying assumptions of this model.

We have presented the first quantitative, spatially resolved measurements of elastic strains within dislocation cells. These measurements provide critical data for validating and guiding the development of detailed dislocation-based simulations and models for every major facet of dislocation structure evolution and dislocation transport.

METHODS

Tensile and compression specimens were prepared from ⟨001⟩-oriented 99.999+% Cu single crystals. The compression sample was cylindrical with nominal dimensions of 10 mm in diameter by 20 mm in length. The tension sample had 10-mm-diameter cylindrical grips and a 10-mm-long gauge section with a 5-mm-wide square cross-section and ⟨001⟩ faces. The compression and tensile samples were deformed to relatively large final true flow stresses of ≈200 MPa at true strains of ≈30%. All X-ray measurements were made on samples cut (with an acid saw) from regions as close as possible to the centre of the original gauge section.

The spatially resolved scanning monochromatic DAXM measurements were conducted using an X-ray microbeam focused to ≈0.5 μm (refs 31,32) by crossed Kirkpatrick–Baez focusing mirrors using the XOR/UNI beamline 34-ID at the APS. Figure 1 is a schematic illustration of the diffraction geometry in which diffracted X-ray beams from a (energy scanning) monochromatic incident microbeam are detected using a CCD area X-ray detector; depth resolution is provided by a 50-μm-diameter platinum wire diffracted-beam

©2006 Nature Publishing Group

profiler as described previously in connection with elastic strain measurements in cylindrically bent silicon (ref. 30). In this method, a two-dimensional depth versus energy scan is carried out to determine the Bragg energy and Bragg angle for scattering from a particular sharp peak in the CCD image. For depth, the profiling wire is step-scanned parallel to the sample surface in a knife-edge fashion using 0.7-μm steps (that is, 0.5 μm along the beam). This sequentially blocks diffracted beams that were incident on individual pixels of the CCD and allows the origin (along the microbeam) of the diffracted X-rays to be determined in all three dimensions with an accuracy of ≈0.5 μm by triangulation[31,32]. For each wire position, the energy is scanned through the peak in 2 eV steps to determine the energy and depth at which the intensity is a maximum; the energy at the peak corresponds to the Bragg energy of the dislocation cell and the Bragg angle is determined from the microscope calibration using the depth of the peak intensity and the pixel position of the depth-resolved diffraction peak on the CCD. The X-ray energy, $E \approx 14$ keV, used in these experiments made it possible to obtain data from sample depths up to ≈50 μm.

The depth-resolved intensity versus energy curve shown in the inset depth–energy plot in Fig. 2 corresponds to a $\Delta E/E = \Delta q/q$ profile for an individual dislocation cell, which in turn directly provides the $\Delta q/q$ peak positions in Fig. 2a,b. We note that the diffraction width for the cell interior is quite sharp, as the full-width at half-maximum of the peak in the inset corresponds to $\Delta E/E = \Delta q/q \approx 3 \times 10^{-4}$ or about one-third of the smallest tick spacing in Fig. 2. This is not much larger than our intrinsic energy width of ≈3 eV (including the microbeam convergence[30]), which gives an instrumental resolution of $\Delta q/q \approx 2 \times 10^{-4}$ for the experimental conditions[30]. We note that these data were intended to measure peak positions and are not adequate for resolving detailed peak shapes.

Received 31 March 2006; accepted 21 June 2006; published 16 July 2006.

References

1. Kubin, L. in *Dislocation Patterning* (eds Cahn, R. W., Haasen, P. & Kramer, E. J.) 137–190 (Mughrabi, H. (Vol. ed) Materials Science and Technology, Vol. 6, VCH, Weinheim, 1993).
2. Sevillano, J. G. in *Flow Stress and Work Hardening* (eds Cahn, R. W., Haasen, P. & Kramer, E. J.) 19–88 (Mughrabi, H. (Vol. ed.) Materials Science and Technology, Vol. 6, VCH, Weinheim, 1993).
3. Gómez-García, D., Devincre, B. & Kubin, L. P. Dislocation patterns and the similitude principle: 2.5D mesoscale simulations. *Phys. Rev. Lett.* **96,** 125503 (2006).
4. Argon, A. S. & Haasen, P. A new mechanism of work hardening in the late stages of large strain plastic flow in f.c.c. and diamond cubic crystals. *Acta Metall. Mater.* **41,** 3289–3306 (1993).
5. Thomson, R. & Levine, L. E. Theory of strain percolation in metals. *Phys. Rev. Lett.* **81,** 3884–3887 (1998).
6. Levine, L. E. & Thomson, R. The statistical origin of bulk mechanical properties and slip behavior in fcc metals. *Mater. Sci. Eng. A* **400–401,** 202–205 (2005).
7. Kassner, M. E., Perez-Prado, M.-T., Vecchio, K. S. & Wall, M. A. Determination of internal stresses in cyclically deformed copper single crystals using convergent-beam electron diffraction and dislocation dipole separation measurements. *Acta Mater.* **48,** 4247–4254 (2000).
8. Hu, X., Wei, C., Margolin, H. & Nourbakhsh, S. Bauschinger effect and the stresses in a strained single crystal. *Scr. Metall. Mater.* **27,** 865–870 (1992).
9. Hasegawa, T., Yakou, T. & Kocks, U. F. A unified representation of stress-strain curves in reversed direction of prestrained cell-forming metals. *Trans. Japan Inst. Met.* **27,** 425–433 (1986).
10. Ungár, T., Mughrabi, H., Rönnpagel, D. & Wilkens, M. X-ray line-broadening study of the dislocation cell structure in deformed [001]-orientated copper single crystals. *Acta Metall.* **32,** 333–342 (1984).
11. Mughrabi, H., Ungár, T., Kienle, W. & Wilkens, M. Long-range internal stresses and asymmetric X-ray line-broadening in tensile-deformed [001]-oriented copper single crystals. *Phil. Mag. A* **53,** 793–813 (1986).
12. Ungár, T. & Borbély, A. The effect of dislocation contrast on x-ray line broadening: a new approach to line profile analysis. *Appl. Phys. Lett.* **69,** 3173–3175 (1996).
13. Ungár, T., Groma, I. & Wilkens, M. Asymmetric X-ray line broadening of plastically deformed crystals. II. Evaluation procedure and application to [001]-Cu crystals. *J. Appl. Crystallogr.* **22,** 26–34 (1989).
14. Wilkens, M., Herz, K. & Mughrabi, H. An X-ray diffraction study of cyclically and of unidirectionally deformed copper single crystals. *Z. Metallkd.* **71,** 376–384 (1980).
15. Straub, S. *et al.* Long-range internal stresses in cell and subgrain structures of copper during deformation at constant stress. *Acta Mater.* **44,** 4337–4350 (1996).
16. Mughrabi, H. Dislocation wall and cell structures and long-range internal stresses in deformed metal crystals. *Acta Metall.* **31,** 1367–1379 (1983).
17. Hähner, P., Bay, K. & Zaiser, M. Fractal dislocation patterning during plastic deformation. *Phys. Rev. Lett.* **81,** 2470–2473 (1998).
18. Zaiser, M. A generalized composite approach to the flow stress and strain hardening of crystals containing heterogeneous dislocation distributions. *Mater. Sci. Eng. A* **249,** 145–151 (1998).
19. Zaiser, M. & Hähner, P. The flow stress of fractal dislocation arrangements. *Mater. Sci. Eng. A* **270,** 299–307 (1999).
20. Hähner, P. & Zaiser, M. Dislocation dynamics and work hardening of fractal dislocation cell structures. *Mater. Sci. Eng. A* **272,** 443–454 (1999).
21. Krivoglaz, M. A. & Ryaboshapka, K. P. Theory of X-ray scattering by crystals containing dislocations, screw and edge dislocations randomly distributed throughout the crystal. *Fiz. Metal. Metalloved.* **15,** 18–31 (1963) Engl. transl: *Phys. Metals Metallogr.* **15**, 14–26 (1963).
22. Wilkens, M. The determination of density and distribution of dislocations in deformed single crystals from broadened X-ray diffraction profiles. *Phys. Status Solidi A* **2,** 359–370 (1970).
23. Levine, L. E. & Thomson, R. X-ray scattering by dislocations in crystals. General theory and application to screw dislocations. *Acta Crystallogr. A* **53,** 590–602 (1997).
24. Groma, I. X-ray line broadening due to an inhomogeneous dislocation distribution. *Phys. Rev. B* **57,** 7535–7542 (1998).
25. Jakobsen, B. *et al.* Formation and subdivision of deformation structures during plastic deformation. *Science* **312,** 889–892 (2006).
26. Ungár, T. Characteristically asymmetric X-ray line broadening, an indication of residual long-range internal stresses. *Mater. Sci. Forum* **166–169,** 23–44 (1994).
27. Ungár, T., Mughrabi, H., Wilkens, M. & Hilscher, A. Long-range internal stresses and asymmetric X-ray line-broadening in tensile-deformed [001]-oriented copper single crystals: the correction of an erratum. *Phil. Mag. A* **64,** 495–496 (1991).
28. Borbély, A., Blum, W. & Ungar, T. On the relaxation of the long-range internal stresses of deformed copper upon unloading. *Mater. Sci. Eng. A* **276,** 186–194 (2000).
29. Larson, B. C., Yang, W., Ice, G. E., Budai, J. D. & Tischler, J. Z. Three-dimensional X-ray structural microscopy with submicrometre resolution. *Nature* **415,** 887–890 (2002).
30. Yang, W. *et al.* Spatially resolved Poisson strain and anticlastic curvature measurements in Si under large deflection bending. *Appl. Phys. Lett.* **82,** 3856–3858 (2003).
31. Yang, W. *et al.* Differential-aperture X-ray structural microscopy: a submicron-resolution three-dimensional probe of local microstructure and strain. *Micron* **35,** 431–439 (2004).
32. Ice, G. E. *et al.* Polychromatic X-ray microdiffraction studies of mesoscale structure and dynamics. *J. Synchrotron Radiat.* **12,** 155–162 (2005).
33. Ledbetter, H. M. & Naimon, E. R. Elastic properties of metals and alloys. II. Copper. *J. Phys. Chem. Ref. Data* **3,** 897–935 (1974).

Acknowledgements

M.E.K. and M.D.R. acknowledge support from the Office of Basic Energy Sciences (BES), DoE, and thank the National Center for Electron Microscopy at LBNL for access to the TEM. Research at ORNL is supported by DoE BES Division of Materials Sciences under contract with UT-Battelle, LLC. The XOR/UNI facilities on sectors 33 and 34 at the APS are supported by the US DoE, Office of Science. Correspondence and requests for materials should be addressed to L.E.L.

Competing financial interests

The authors declare that they have no competing financial interests.

Reprints and permission information is available online at http://npg.nature.com/reprintsandpermissions/

©2006 Nature Publishing Group